A novel CO-tolerant PtRu core–shell structured electrocatalyst with Ru rich in core and Pt rich in shell for hydrogen oxidation reaction and its implication in proton exchange membrane fuel cell

Lei Zhang [a,*], Jenny Kim [a], Hao Ming Chen [b], Feihong Nan [c], Karleen Dudeck [c], Ru-Shi Liu [b], Gianluigi A. Botton [c], Jiujun Zhang [a]

[a] Institute for Fuel Cell Innovation, National Research Council Canada, Vancouver BC, V6T 1W5, Canada
[b] Department of Chemistry, National Taiwan University, Taipei 106, Taiwan
[c] Dept of Materials Science and Engineering, McMaster University, Ontario L8S 4M1, Canada

ABSTRACT

A novel PtRu catalyst consisting of a Ru-rich core and a Pt-rich shell was synthesized using a two-step microwave irradiation technique. The synthesized PtRu/C catalysts were characterized by X-ray diffraction (XRD), extended X-ray absorption finestructure (EXAFS), transmission electron microscopy (TEM) as well as energy dispersive X-ray spectrometry (EDXS). The produced PtRu/C catalysts showed identical crystalline structure and diffraction peaks to Pt itself, but with negligible higher 2 shift degrees, indicating the formation of a specific composite structure rather than alloy formation. This novel structure of PtRu/C catalyst was also further verified via X-ray absorption spectroscopy. The particle size of PtRu catalysts identified by TEM was less than 5 nm. In order to investigate the CO tolerance in the hydrogen oxidation reaction (HOR), H_2 streams with six different concentrations of CO (0, 10, 50, 100, 300, and 500 ppm) were used. The electrocatalytic activity thus obtained was not only better than that of Pt/C catalyst in HOR, but also showed a better CO tolerance in various CO concentrations.

Crown Copyright © 2011 Published by Elsevier B.V. All rights reserved.

1. Introduction

Proton exchange membrane (PEM) fuel cells have several advantages such as high energy density, high power density, high-energy conversion efficiency as well as low/zero emission, and have been recognized as the promising energy conversion devices in many applications such as portable electronic devices, residential power systems, and transportation vehicles. For a typical hydrogen (H_2)–oxygen (O_2 from air) fuel cell, the H_2 fuel is oxidized at the anode catalyst layer (Pt-based catalyst) to release electrons and protons, and O_2 is reduced at the cathode catalyst layer (Pt-based catalyst) by accepting the incoming electrons and the protons from the anode to produce power through the external load, and at the same time to produce water and heat as well. In the current state of technology, hydrogen fuel mainly comes from steam reforming of hydrocarbons [1,2]. Unfortunately, this reformed hydrogen contains significant amount of impurities such as CO and CO_2, which, in particular for CO, could poison the anode Pt catalyst, leading to significant fuel cell performance degradation. Therefore, developing Pt-based anode catalysts with CO tolerance has been becoming one of the important tasks in PEM fuel cell development and commercialization.

In current PEM fuel cell technology, the most practical catalysts are Pt-based catalysts for both anode hydrogen oxidation reaction (HOR) and cathode oxygen reduction reaction (ORR). Unfortunately, if Pt-based catalysts are used for HOR at anode, CO contaminating the hydrogen fuel will be easily adsorbed on Pt particle surface, degrading its catalytic activity for H_2 oxidation, leading to significant drop in fuel cell performance even in the presence of as low as 25 ppm CO concentration [3].

In order to reduce this negative impact of CO on anode catalyst, great efforts have been made in the past two decades. One of the approaches is to develop novel anode catalysts, which have high CO tolerance. The most feasible one is the bimetallic heterogeneous catalyst such as carbon-supported Pt–Ru alloy catalysts. In recent years, Pt-based core–shell structured catalysts with Ru as the core and Pt as the shell (Ru@Pt) have been widely explored [4–7]. These materials show much enhanced CO oxidation activity when compared to PtRu alloy and monometallic Pt and Ru nanoparticle catalysts, leading to improved CO tolerance capability. Recent studies also revealed that carbon-supported Ru@Pt catalysts could catalyze preferential oxidation of adsorbed CO on the

Pt surface in order to quickly release active sites occupied by CO, resulting in an improved hydrogen oxidation reaction in the presence of CO in the fuel feed stream. Due to the fact that Ru metal is confined and kinetically trapped inside a Pt shell, the conventional bi-functional mechanism may not be applied to explain this increased CO removal. Using Density Functional Theory, Alayoglu et al. [4] showed that the enhanced CO oxidation may be achieved through the interactions between the Pt shell and Ru core atoms, which can modify the electronic structure of the Pt surface by the presence of subsurface Ru atoms. This modification may significantly destabilize CO on Pt, leading to a lower CO saturation coverage, thereby providing more free active sites for hydrogen oxidation reaction.

With respect to the synthesis of Pt–Ru bimetallic catalysts, there are several methods including breaking metal clusters into nanoscale metal particles [8] and aggregating metal atoms into nanoscale metal particles [9–17]. Among these techniques, the microwave irradiation method [18,19] was recently applied for the synthesis of bimetallic heterogeneous catalysts due to the uniform reduction of metals that can be achieved in a short time period. With this method, a homogeneous particle size distribution could also be achieved by uniformly heating the particles. Therefore, the microwave method is considered one of the effective methods for easy and quick synthesis of catalysts.

In the effort to develop novel CO-tolerant catalysts for the anode hydrogen oxidation reaction in PEM fuel cells, we recently synthesized a novel bimetallic heterogeneous PtRu electrocatalyst with a structure consisting of a Ru rich in core with a Pt rich shell using a two-step microwave irradiation technique. In order to analyze the catalyst morphology and characterize the bimetallic catalysts structure and composition, we have used X-ray diffraction (XRD), transmission electron microscopy (TEM) and scanning transmission electron microscopy (STEM), X-ray absorption spectroscopy (XAS) [20–22], as well as extended X-ray absorption fine structure (EXAFS) in order to provide structural information on the synthesized materials. Using these techniques, particles with a Ru rich in core and Pt rich in shell structure were successfully identified. Our results indicate that these particles are different from those core–shell structured Pt–Ru catalysts reported in the literature. For CO-tolerance testing purposes, this novel nanostructured Pt–Ru catalyst was used to prepare the membrane-bonded anode catalyst layer and then assembled into an in-house half-cell for measurements in the presence of CO in the hydrogen feeding stream. Experiments showed that this novel structured catalyst have strong CO-tolerance capability when compared to that of commercially available Pt–Ru alloy catalyst.

2. Experimental

2.1. Synthesis of Ru rich in core and Pt rich in shell structured PtRu/C electrocatalyst

For synthesizing a Ru-rich core and Pt-rich shell structured Pt–Ru catalyst supported on carbon, ruthenium (III) acetylacetonate (97% Ru(acac)$_3$, Sigma–Aldrich) was first reduced in tetra (ethylene glycol) solution (99% t-EG, Sigma–Aldrich) in a microwave oven for a certain time, and platinum (II) chloride ($\geq$99.99% PtCl$_2$, Sigma–Aldrich) and carbon black (Vulcan-XC-72R) were added into it (molar ratio between Pt and Ru was 1:1, and the total metal loading was 20-wt%) under constant stirring overnight to form a slurry mixture. This mixture was then further reduced in the microwave oven for a certain time. The mixture slurry was then treated in a high-speed centrifuge (Thermo Scientific Sorvall Legend RT+ Centrifuge, Sorvall) to separate the catalyst particles from the solvent, followed by ethanol rinse by several times in order to wash and remove any residues on the catalyst particles. After dried

in the oven overnight at 100 °C, the final product was ground in a mortar into powder for physical and electrochemical characterization. Note that this carbon supported catalyst is expressed as PtRu/C in this article, and composition was expected to have molar and weight ratios of 2:1 and 1:1 (Pt/Ru), respectively, later confirmed through the characterization techniques.

2.2. Catalyst material characterization using instrument methods

The structure and phase analysis of PtRu/C catalysts obtained above were conducted via XRD (D8 ADVANCE X-ray diffractometer, Bruker Axs, Inc.) with Cu $K_{\alpha 1}$ radiation. The XRD pattern was recorded between 20° and 90° with a scan speed of 0.1 s/step and increment of 0.02°/step at current and voltage of 40 mA and 40 kV, respectively. The morphology and particle size of the catalyst was analyzed using a transmission electron microscope (Tecnai G^2-F20 High-Resolution TEM), and the composition qualitative analysis was conducted by EDX (Link Isis System, Oxford, Hitachi S-3500N). For a more detailed analysis of the catalyst structure and composition distribution over larger sample areas as well as for individual particle measurements, analytical measurements were conducted by EDX combined with STEM in an aberration corrected microscope (FEI Titan 80–300 cubed) equipped with a high-brightness electron source capable of achieving sub 0.1 nm probe size and a high-angle annular dark-field detector (HAADF) for "atomic number" contrast imaging. The extended X-ray absorption fine structure (EXAFS) technique was also employed as a short-range probe of structure for PtRu/C catalyst, providing information on local correlations around the absorbing atom. In this respect, a series of EXAFS measurements of the synthesized samples were made using synchrotron radiation at room temperature. The measurements were made at the Pt L$_3$ edge (11,564 eV) and the Ru K edge (22,117 eV). For EXAFS measurements, the backscattering amplitude and phase shift functions for specific atom pairs were calculated *ab initio* using the FEFF7 code. X-ray absorption data were analyzed using standard procedures, including pre-edge and post-edge background subtraction, normalization with respect to edge height, Fourier transformation and nonlinear least-squares curve fitting. The normalized k^3-weighted EXAFS spectra, $k^3 x(k)$, were Fourier-transformed in a k range from 2.5 to 12 Å^{-1}, to evaluate the contribution of each bond pair to the Fourier transform (FT) peak. The experimental Fourier-filtered spectra were obtained by performing an inverse Fourier transformation with a Hanning window function with r between 1.6 and 3.1 Å. The S_0^2 (amplitude reduction factor) values of the Ru and Pt atoms were fixed at 0.81 and 0.83, to determine the structural parameters of each bond pair. Ru and Pt edge data were analyzed simultaneously.

2.3. Catalyst ink preparation for catalyst layer

The developed PtRu/C catalyst above was used to prepare catalyst ink. The amount of 40 mg of 20-wt% PtRu/C powder was mixed with DI water (18.1 Mohm purity, MilliQ Ultra-High Water, MILLIPORE) followed by the addition of 2-propanol (IPA, Fisher Scientific). While stirring of this mixture, a certain amount of 1 wt% Nafion® solution (diluted solution from 5% (w/w) perfluorosulfonic acid-PTFE copolymer–alcohol solution using DI water) was added dropwise to the catalyst mixture. After adding IPA, a probe sonicator (Sonicator 3000, MISONIX) was submerged into this mixture for 30 min of intermittent sonication (pulse on: 1 min, pulse off: 30 s, initial output: 5.0 W).

2.4. Preparation of Catalyst layer membrane electrode assembly

For catalyst layer preparation, a piece of 5.5 cm by 6.5 cm of 3 M adhesive films was pre-cut. At the center of this film, there were two

3.0 mm by 3.0 mm square holes which were cut off with a distance of 6.5 mm apart from each other. This film was then attached on the top of a Teflon transfer sheet (11.2 cm by 11.2 cm). In controlling the catalyst loading, the Teflon sheet substrate was weighed before ink spraying, and then placed on the top of a hot plate. A stainless steel plate (10.0 cm by 10.0 cm) with an exposed area of 1.0 cm by 2.5 cm at the center was put onto the Teflon sheet to regulate the spraying area to be 2.5 cm². The prepared 20-wt% PtRu/C catalyst ink was then poured into a 60 mL syringe (BD Luer-Lock, Becton Dickinson and Company), and the syringe was placed into an automatic infusion device (NE-1600 6-Syringe Pump, New Era Pump Systems, Inc.) which was connected to the spray machine (VXM Stepping Motor Controller, Velmex, Inc.). The temperature of hot plate and infusing rate of ink were set at 75 °C and 10 mL h⁻¹, respectively. The weight of catalyst coated Teflon sheet was measured after a certain amount of catalyst ink was infused and cooled down. The catalyst ink spraying process was repeated until the targeted 2.0 mg cm⁻² catalyst loading was achieved.

For preparation of membrane electrode assembly, the Teflon sheet coated with catalyst layer was cut/scratched into pieces of 1 mm × 1 mm surface area reaching the target catalyst layer area of 1 mm². This 1 mm² of catalyst layer coated on Teflon sheet was then cast onto the center of a gas diffusion layer (GDL) disk, which had 2.7 cm diameter. Then a 4 cm × 4 cm of Nafion® 211 membrane was placed on the top of the catalyst layer, and subsequently this sandwich assembly was put into a bonding machine (Standard Automatic Bench Top Press 3893 (Four-post Model), Carver, Inc.) to form a membrane electrode assembly at 135 °C and 2300 lb pressure for 2.5 min.

2.5. Electrochemical measurements

The electrochemical measurements for hydrogen oxidation reaction catalyzed by developed PtRu/C catalyst in this work and the corresponding CO tolerance were conducted using an in-house designed electrochemical half-cell and bipotentiostat (AFCBP1, PINE Instrument Company) with associated software (PineChem). This half-cell was designed to allow the hydrogen gas or the mixed gas of hydrogen and CO blowing into the anode channel to reach the GDL side. On the cathode side, a Pt wire inset into the electrolyte served as the counter electrode, and a saturated calomel electrode (SCE), also located in the same side as counter electrode, was used as the reference electrode. A 0.5 M H₂SO₄ aqueous solution was used as the electrolyte. During the measurements, this half-cell was first purged with N₂(g) gas to remove any residual air. The gas supply was then changed from N₂ to H₂ or the mixed gas of H₂ and CO. Subsequently, the linear sweep voltammetry (LSV) was scanned with a potential scan rate of 20 mV s⁻¹ in the range of −0.3 to 1.5 V vs. SCE. The final cell resistance (Ω) was recorded again. The mixed gas of H₂ and CO contained 10, 50, 100, 300, and 500 ppm CO, respectively. All electrochemical measurements were done at room temperature and atmospheric pressure.

3. Results and discussions

3.1. Physical characterization of the prepared PtRu/C catalysts

The structure and phase analysis of PtRu/C catalyst was conducted by XRD as shown in Fig. 1, together with other diffractograms obtained from different types of electrocatalysts for comparison. Fig. 1(a) shows the XRD spectrum of commercially available 20-wt% Pt supported on carbon. In Fig. 1(b), the diffractogram of commercially available 20-wt% Pt–Ru alloy on carbon is shown. The XRD spectrum of in-house synthesized 20-wt% PtRu deposited on carbon by the microwave irradiation method
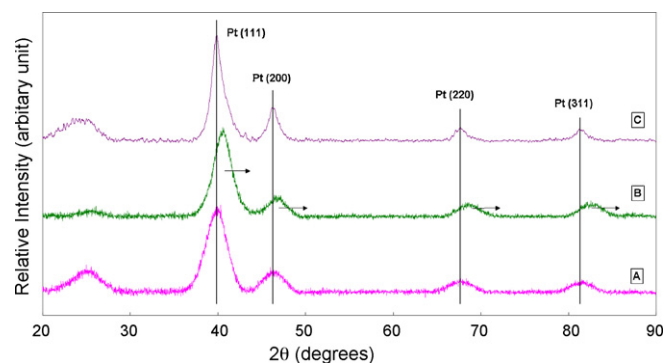
Fig. 1. X-ray diffractograms of the electrocatalysts: (a) commercially available 20-wt% Pt/C, (b) commercially available 20-wt% Pt–Ru alloy/C, and (c) in-house synthesized 20-wt% PtRu/C.

is shown in Fig. 1(c). The diffraction peak at $2\theta = 25°$ represents (0 0 2) plane diffraction of hexagonal Vulcan XC-72R carbon support, and the solid vertical lines represent standard (1 1 1), (2 0 0), (2 2 0), and (3 1 1) reflections for pure Pt. It can be seen that all XRD spectra predominantly exhibit the characteristics of a single-phase face-centered cubic (FCC) crystalline structure. Compared to the commercially available 20-wt% of Pt/C catalyst (Fig. 1(a)), the diffraction peaks of the commercially available PtRu/C alloy catalyst (Fig. 1(b)) are shifted to higher angles, indicating the contraction of the lattice due to the formation of alloying of Ru with Pt. However, instead of shifting to higher degrees, the diffraction peaks of the in-house synthesized 20-wt% PtRu/C catalysts (Fig. 1(c)) show the same diffraction peak positions as those of commercially available 20-wt% of Pt/C catalyst without obvious peak shift, indicating that Ru and Pt in PtRu/C catalysts are not in the same alloy state as in commercially available PtRu alloy catalyst. To further characterize these nanostructures, TEM, STEM and EXAFS analysis were carried out and the results are shown in the later section. Based on (2 2 0) XRD reflection, the particle size of the synthesized PtRu/C catalyst was calculated. The mean particle size obtained was about 5–6 nm.

In order to verify the efficiency and repeatability of the two-step microwave irradiation method, the catalyst synthesis was repeated three times. The obtained compositions, both by wt% and at%, were determined by EDX and were listed in Tables 1 and 2. In addition, to

Table 1
Weight composition of 20-wt% PtRu/C catalysts prepared by the two-step microwave irradiation method.

	Synthesis #1		Synthesis #2		Synthesis #3	
	Ru	Pt	Ru	Pt	Ru	Pt
Weight (%) in the carbon-supported catalysts						
Location #1	7.43	17.9	7.49	14.86	6.26	14.02
Location #2	8.31	19.33	7.71	14.51	6.65	15.31
Location #3	8.45	18.85	8.32	15.08	6.66	14.15
Average (wt%)	8.06	18.69	7.84	14.82	6.52	14.49

Table 2
Atomic composition of 20-wt% PtRu/C catalysts prepared by the two-step microwave irradiation method.

	Synthesis 1		Synthesis 2		Synthesis 3	
	Ru	Pt	Ru	Pt	Ru	Pt
Atomic (%) in the carbon-supported catalysts						
Location #1	1.15	1.44	1.12	1.15	0.91	1.06
Location #2	1.32	1.60	1.15	1.12	0.99	1.18
Location #3	1.34	1.55	1.26	1.18	0.98	1.08
Average (at%)	1.27	1.53	1.18	1.15	0.96	1.11
Average ratio of Ru:Pt	1:1.2		1:0.97		1:1.2	
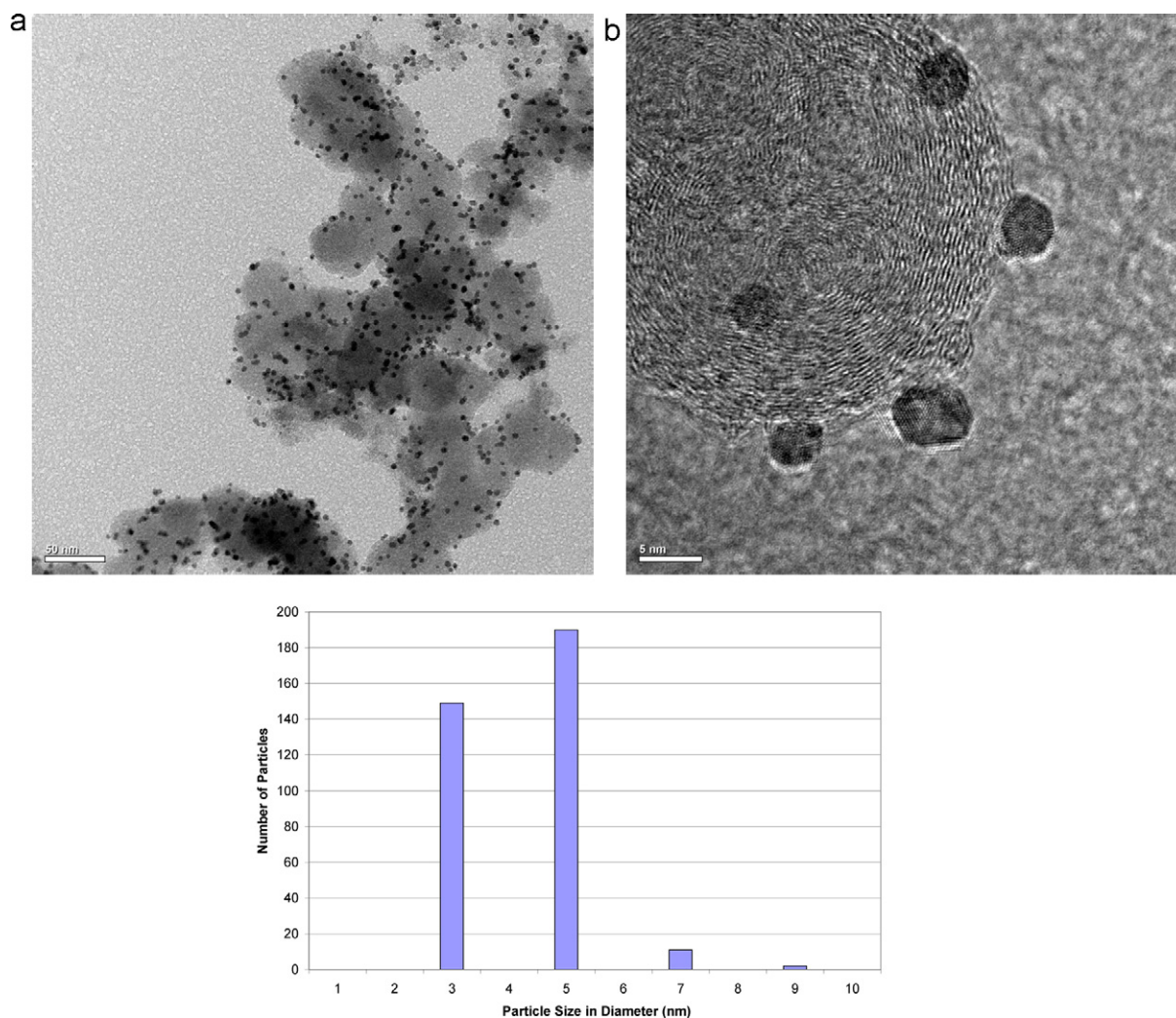
Fig. 2. (a) Conventional TEM micrograph of 20-wt% PtRu catalysts supported on carbon. (b) Low-resolution micrograph of 20-wt% PtRu/C catalysts. (c) Prepared 20-wt% PtRu/C nanoparticle size distribution histogram.

validate the homogeneity of the composition distribution of Pt and Ru in the prepared PtRu/C catalysts, three different locations across each catalyst sample were randomly selected and compared to get an average composition, as shown in Tables 1 and 2 as well. It can be clearly seen from Tables 1 and 2 that the average Ru:Pt ratios of three-batch synthesis is relatively uniform, and corresponding to ~1:1 by atom, demonstrating that the efficiency and repeatability of the two-step microwave irradiation method are high enough. This atomic ratio is also consistent with the originally designed composition of Pt and Ru.

The morphology of 20-wt% PtRu catalysts supported on carbon as determined from TEM imaging together with EDX analysis was also shown in Fig. 2(a) and (b). It can be seen from Fig. 2(a) that the catalyst particles (dark particles) are well and uniformly dispersed on the surface of carbon particles. The high magnification images (Fig. 2(b)) clearly show that the catalyst particles have an average particle size of around ~5 nm with a dominantly spherical shape. These sphere particles are uniformly deposited onto a larger carbon particle. The catalyst particle size distribution of around 2.5–4.5 nm is shown by the histogram in Fig. 2(c). This is consistent with the results obtained from XRD measurement as shown in Fig. 1. In order to test local variations in composition within the particles, STEM HAADF imaging and EDX mapping over individual particle as well as larger sample area were carried out. Fig. 3(a) shows STEM HAADF images as well as EDX analysis, from the PtRu supported on carbon

sample. Characterization results indicate that catalyst nanoparticles with a structure of Pt/Ru ratio varying from the shell to the core were synthesized. According to the elemental analysis results, it is also obvious that Pt/Ru ratio varies from shell to core. HAADF images also show that the shell is generally brighter than the core, suggesting higher atomic number atoms are located on the shell of the nanoparticles.

EDXS mapping was also performed over individual nanoparticles. Result shown in Fig. 3(b) indicates the variation of Ru and Pt from shell to the core area. Furthermore, for a typical PtRu nanoparticle supported on carbon, it appears clearly that Ru is mainly distributed in the core area, while Pt distributed in both areas but with higher ratio in the shell consistent with nanoparticles fully covered with Pt. Since the electrons travel through the top and bottom surfaces as well as the core of the particle when the electron beam is placed in the center of the particle, Pt signal from the top and bottom surfaces is also detected. Nanoparticles with triangular shape are also found in the sample, indicating the presence of tetrahedral or triangular prism shape. According to the EDXS mapping results in Fig. 3(c) and HAADF imaging, it is very clear that nanoparticle with a Ru rich core and Pt rich shell were obtained from the synthesis route.

To gain further insight on the local structure of the synthesized PtRu/C nanoparticles, EXAFS analyses were also performed. Fig. 4 shows the Fourier transform of the EXAFS oscillations of
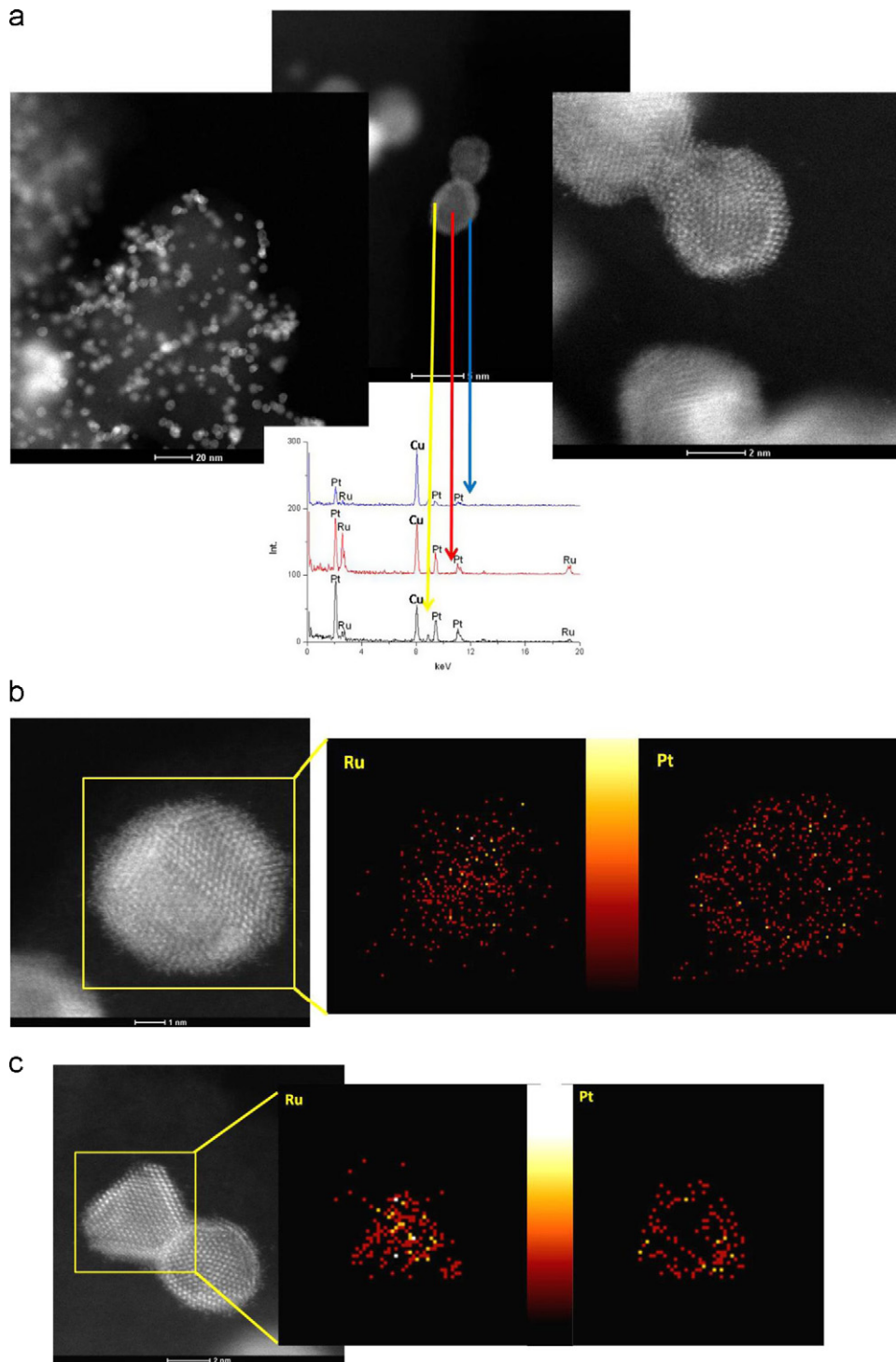
Fig. 3. (a) STEM HAADF images as well as EDXS point spectra from the core and shell for PtRu catalysts supported on carbon. The Cu signal arises from the support grid background. (b) HAADF (left) and EDX mapping (Ru and Pt maps) over a typical RuPt nanoparticle. (c) HAADF image (left) and EDX mapping (Ru and Pt maps) over the RuPt nanoparticle with triangular projected shape.

Pt L_3-edge for the PtRu/C sample and corresponding Pt foil baseline reference spectrum. Most interestingly, the peak position of PtRu/C sample is located in lower range than that of the pure Pt reference foil, indicating that the first shell around the Pt atoms included neighbouring atoms of two elements. With regard to the Ru atoms environment, the Fourier transform of the EXAFS oscillations (Fig. 5) of PtRu/C before phase correction showed a strong peak at ~2.4 Å but with a shoulder at ~2.1 Å, which made this strong peak asymmetry, indicating that the first shell around the Ru atoms included neighbouring atoms of two elements as well. The peak at ~2.4 Å is assigned to single scattering by Ru–Ru atoms and the shoulder at ~2.1 Å corresponds to a single scattering by the Ru–Pt atoms. This result is characteristic of the co-existing of the Pt–Ru system, implying that some Ru atoms diffused into the Pt particles, and vice versa. This phenomenon is consistent with the STEM HAADF observation and EDXS point analysis and mapping
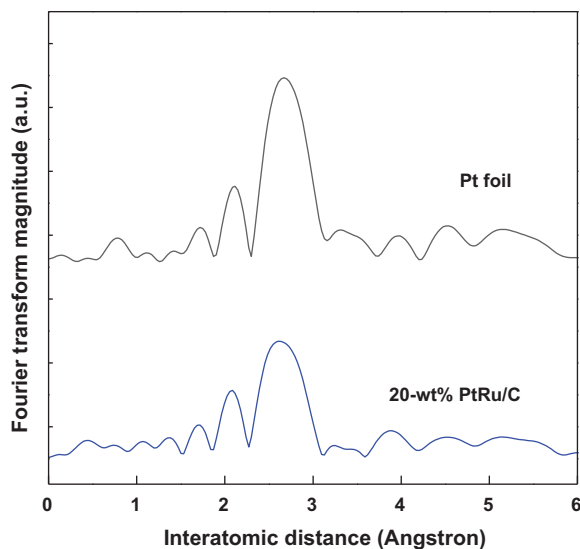
Fig. 4. Fourier transform of EXAFS oscillations of Pt L$_3$-edge for PtRu/C catalysts and corresponding foil.

in Fig. 3. As a result, we can see that our PtRu/C catalysts have a possible structure of a Ru-rich core and a Pt-rich shell. From the Ru@Pt nanoparticle center to its surface, the Pt density is gradually increased and the Ru density is gradually decreased. This is the major difference of this PtRu/C core–shell structured nanoparticle from that of traditional Ru–Pt core shell structure, where the core is fully consisted of Ru, and the shell is composed of 1–2 monolayers of Pt [4].

On the other hand, the main XRD peak located at around 40° in Fig. 1 shows some asymmetry. This effect might be resulting from the incorporation of Ru atoms with Pt although we cannot find any resolvable diffraction peaks from Ru crystals in Fig. 1. A Ru core, too small to diffract coherently, might be one possible reason for the undetectable Ru diffraction peaks by XRD.

3.2. Catalytic activity toward hydrogen oxidation reaction (HOR)

The HOR catalytic activity of in-house synthesized core–shell structured PtRu/C catalyst was tested using the in-house designed
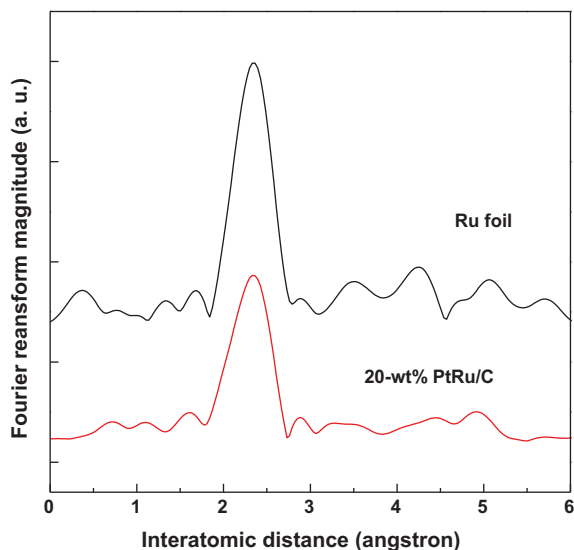
Fig. 5. Fourier transform of EXAFS oscillations of Ru K-edge for PtRu/C catalysts and corresponding Ru reference foil.
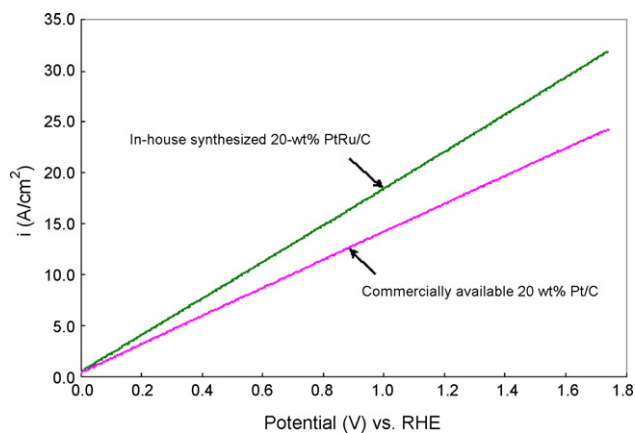
Fig. 6. Polarization curves of commercially available 20-wt% Pt/C and the developed PtRu/C catalysts for hydrogen oxidation reaction obtained in 0.5 M H$_2$SO$_4$(aq) at ambient conditions. The potential scan rate and flow rate of hydrogen stream were 20 mV s^{-1} and 5 mL min^{-1}, respectively. Catalyst loading: 2 mg cm^{-2}.
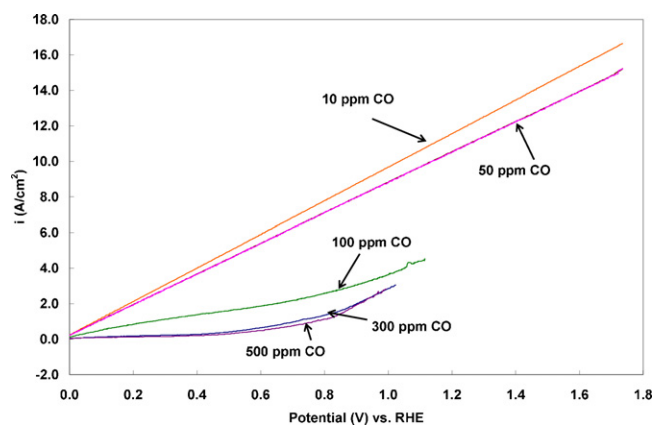
Fig. 7. Polarization curves for CO tolerance of the prepared 20-wt% PtRu/C core–shell catalyst. The experiment conditions are the same as in Fig. 6.

electrochemical half-cell. The HOR polarization curve was obtained in 0.5 M H$_2$SO$_4$ solution at ambient conditions with H$_2$ feeding, as shown in Fig. 7. For comparison, the electrode catalyzed by a commercially available 20-wt% Pt/C catalyst was also plotted in this figure. From Fig. 6, it can be clearly seen that in the current density region studied, the developed PtRu/C catalyst shows much better HOR catalytic activity than that of commercially available Pt/C catalyst. The overpotentials measured from both catalysts at a current density of 1.0 A cm^{-2} are summarized in Table 3.

3.3. CO tolerant capability toward hydrogen oxidation reaction (HOR)

To investigate the CO tolerance of the prepared 20-wt% PtRu/C catalyst, the anode feed gas of H$_2$ containing 10, 50, 100, 300, and 500 ppm CO, respectively, was used as shown in Fig. 7. As the concentration of CO is increased in the H$_2$ stream, the performance is decreased since more CO occupied the active sites on pure Pt particles, leading to higher CO saturation coverage, which inhibits the interactions between the Pt shell and Ru core atoms. However,

Table 3
Overpotentials obtained from 20-wt% Pt/C and the developed PtRu/C catalysts at a current density of 1.0 A cm^{-2}.

Electrocatalysts	Commercial Pt/C	In-house developed PtRu/C
Potential (mV) vs. RHE	45.0	28.6

Table 4
Overpotentials obtained from commercially available Pt/C, PtRu/C and the prepared PtRu/C catalysts at a current density of $1.0\,A\,cm^{-2}$ for various CO concentrations (measured at room temperature and ambient pressure for 60 min CO exposure).

	CO concentration (ppm)				
	10	50	100	300	500
Overpotential (mV) vs. RHE					
Commercial Pt/C	51.9	91.1	479.1	824.6	879.5
Commercial PtRu/C	88.6	140.9	306.9	763.4	822.0
In-house developed PtRu/C	32.8	87.8	253.8	710.3	768.9

when the PtRu/C core–shell catalyst consisting of novel structure of Ru-rich core and Pt-rich shell is used, higher CO tolerance can be achieved, compared to that of both commercial Pt/C and PtRu catalysts in various CO concentrations as shown in Table 4. Due to the fact that Ru metal is confined and kinetically trapped inside a Pt shell, the conventional bi-functional mechanism may not be applied to explain this increased CO removal. Using Density Functional Theory, Alayoglu et al. [4] showed that the enhanced CO oxidation may be achieved through the interactions between the Pt shell and Ru core atoms, which can modify the electronic structure of the Pt surface by the presence of subsurface Ru atoms or by disrupting the Pt surface arrangement. This modification may significantly destabilize CO on Pt, leading to a lower CO saturation coverage, thereby providing more free active sites for hydrogen oxidation reaction.

4. Conclusions

A carbon-supported 20-wt% PtRu/C electrocatalyst with a novel structure was synthesized using the two-step microwave irradiation technique. Its structural morphology as well as electrocatalytic activity toward the hydrogen oxidation reaction (HOR) was characterized by XRD, TEM, EDXS, EXAFS as well as electrochemical measurements. The PtRu/C catalyst had a single-phase face-centered cubic (FCC) crystalline structure with weight ratio of 2.2:1 (Pt/Ru) and atomic ratio of 1.1:1 (Pt/Ru), and the metal catalyst had a novel structure with Ru-rich core, and decreasing Ru concentration toward a Pt-rich in shell. The carbon monoxide (CO) tolerant capability of this electrocatalyst was investigated using the in-house designed electrochemical half-cell with H_2 anode gas

feedings, which contained five different concentrations of CO (10, 50, 100, 300, and 500 ppm). The performances showed that this synthesized PtRu/C catalyst had better electrocatalytic activity than commercially available 20-wt% Pt/C catalyst in HOR and also had CO tolerance in various CO concentrations.

Acknowledgements

References

[1] F. Besenbacher, I. Chorkendorff, B.S. Clausen, B. Hammer, A.M. Molenbroek, J.K. Nørskov, I. Stensgaard, Science 279 (1998) 1913.
[2] G.W. Huber, J.W. Shabaker, J.A. Dumesic, Science 300 (2003) 2075.
[3] H.-F. Oetjen, V.M. Schmidt, U. Stimming, F. Trila, J. Electrochem. Soc. 143 (1996) 3838.
[4] S. Alayoglu, A.U. Nilekar, M. Mavrikakis, B. Eichhorn, Nat. Mater. 7 (2008) 333.
[5] S. Alayoglu, L.-C. Lai, W.-A. Chiou, B. Eichhorn, Microsc. Microanal. 15 (Suppl. 2) (2009) 1206.
[6] M. Bernechea, S. García-Rodríguez, P. Terreros, E. de Jesús, J. Fierro, S. Rojas, J. Phys. Chem. C 115 (4) (2011) 1287.
[7] H. Gao, S. Liao, J. Zeng, Y. Xie, D. Dang, Electrochim. Acta 56 (2011) 2024.
[8] K.J. Klabunde, Y.-X. Li, B.-J. Tan, Chem. Mater. 3 (1991) 30.
[9] K. Torigoe, K. Esumi, Langmuir 9 (1993) 1664.
[10] K. Esumi, T. Tano, K. Torigoe, K. Meguro, Chem. Mater. 2 (1990) 564.
[11] M.T. Reetz, W. Helbig, J. Am. Chem. Soc. 116 (1994) 7401.
[12] W. Yu, Y. Wang, H. Liu, W. Zheng, J. Mol. Catal. A: Chem. 112 (1996) 105.
[13] T. Kawaguchi, W. Sugimoto, Y. Murakami, Y. Takasu, J. Catal. 229 (2005) 176.
[14] A. Bayrakçeken, A. Smirnova, U. Kitkamthorn, M. Aindow, L. Tŭrker, İ. Eroğlu, et al., J. Power Sources 179 (2008) 532.
[15] M.J. Escudero, E. Hontañón, S. Schwartz, B. Boutonnet, L. Daza, J. Power Sources 106 (2002) 206.
[16] Y. Shao, G. Yin, J. Wang, Y. Gao, P. Shi, J. Power Sources 161 (2006) 47.
[17] Z.L. Liu, J.Y. Lee, W. Chen, M. Han, L.M. Gan, Langmuir 20 (2004) 181.
[18] W. Yu, W. Tu, H. Liu, Langmuir 15 (1999) 6.
[19] A. Bayrakçeken, L. Tŭrker, İ. Eroğlu, Int. J. Hydrogen Energy 33 (2008) 7527.
[20] H.M. Chen, C.F. Hsin, P.Y. Chen, R.S. Liu, S.F. Hu, C.Y. Huang, J.F. Lee, L.Y. Jang, J. Am. Chem. Soc. 131 (2009) 15794.
[21] J.E. Penner-Hahn, Coordin. Chem. Rev. 190 (1999) 1101.
[22] H.M. Chen, C.F. Hsin, R.S. Liu, J.-F. Lee, L.-Y. Jang, J. Phys. Chem. C 111 (2007) 5909.